Available online at www.sciencedirect.com
ScienceDirect
Optics Communications 274 (2007) 85–93
OPTICS COMMUNICATIONS
www.elsevier.com/locate/optcom

Linear and nonlinear coupling properties of a novel multicore circular dielectric waveguide

Ilias Tsopelas *, Yannis Kominis, Kyriakos Hizanidis

National Technical University of Athens, 157 73 Zografou, Athens, Greece

Received 10 November 2006; received in revised form 25 January 2007; accepted 26 January 2007

Abstract

In this work we investigate the linear and nonlinear coupling properties of a novel multicore circular dielectric waveguide. The proposed device consists of a circular central core and many circular sectoral cores at the periphery, while the whole structure can be considered as a nonlinear multicore composite optical coupler. Hybrid guided modes in a circular sectoral dielectric waveguide are derived using circular harmonic expansion for the electromagnetic fields and the Point Matching Method (PMM) for the application of boundary conditions. Several cases are investigated varying some of the parameters of the geometry and the optical frequency in order to produce dispersion diagrams. In advance, the electric and magnetic field distributions for the fundamental guided modes are produced, while linear and nonlinear coupling coefficients as well as the sectoral waveguide mode effective area are derived.

Keywords: Coupler; Sectoral waveguide; Effective area; Guided modes

1. Introduction

During the last decades, optical couplers were studied extensively in the framework of all-optical processing and WDM technology, as they constitute an essential component of lightwave technology. Different classes of coupling devices, such as symmetric and asymmetric, dual-core and multicore, active or passive, composite and birefringent optical couplers, as well as combinations of them, exhibit remarkable optical properties in linear and nonlinear regime [1]. More specifically, directional dual-core symmetric fiber couplers are the most commonly used for a variety of applications related to fiber optics, exhibiting nonlinear optical pulse switching, symmetric and anti-symmetric bright soliton formation [2–4], while asymmetric dual couplers have attracted increasing attention during last years, as they open a new potential in photon management applications offering logic gate operation [5], switching power reduction [6], bound soliton formation [7], as well as robust bistability [3]. Furthermore, dual-core birefringent optical couplers exhibit also remarkable nonlinear optical performance, such as symmetric and anti-symmetric soliton formation [8,9], rocking filter behavior [10], all-optical switching [4], and polarization selectivity [11].

On the other hand, in the context of all-optical data processing and semiconductor laser applications, last years, multicore circular optical couplers–amplifiers have attracted considerable attention by many researchers [12–19], as they seem to be more controllable that their planar counterparts [20–25]. Modeling a nonlinear multicore optical coupler–amplifier, researchers very often use coupled Discrete Nonlinear Schrödinger (DNLS) and Ginzburg-Landau (DGL) equations in which coupling phenomena are represented usually by linear and nonlinear coefficients [2,12,15–18,20–26]. As many works have proved, the knowledge of the range of the value of coupling coefficients, which are mainly determined by the form of the cross-section of the coupler, play an important role over the device linear and nonlinear overall performance.

The purpose of this work is the investigation of the linear and nonlinear coupling properties of a novel

* Corresponding author. Tel.: +30 2107722469; fax: +30 2107723513.
E-mail address: itsop@central.ntua.gr (I. Tsopelas).

0030-4018/$ - see front matter © 2007 Elsevier B.V. All rights reserved.
doi:10.1016/j.optcom.2007.01.065

asymmetric multicore circular dielectric waveguide. The device transverse structure (see Fig. 1) consists of a circular central core and many circular sectoral waveguides (sectoral rings) at the periphery. We consider that linear and nonlinear phenomena are taking place, while the central core material may differ from the sectoral one, rendering the coupler a composite dielectric waveguide [27]. In the literature, the term 'sectoral' (see Fig. 2) was firstly appeared in 1961 [28], and is sometimes confused with ''wedged'' cross-sections even in recent works [29]. Although the investigation of sectoral or wedged waveguide guided modes can be found more in microwave theory concerning metallic structures and filters [29–33] than in optics [34,35], quite recently, in the context of single-mode fiber operation, the so-called segmented-cladding fiber (SCF) – an advanced type of photonic crystal fiber – is analyzed numerically and experimentally as well [36–38]. However, by considering these fibers as couplers, it should be mentioned that the guided mode analysis for the corresponding fiber cross-section, [which resembles to that of our proposed coupler (Fig. 1)], presented in the above-mentioned investigations, is done for the so-called supermodes of the coupling device [1].

In the literature, one may find numerous methods for the modal analysis of optical waveguides of arbitrary cross-section [39,40], such as global (e.g. finite element, finite difference) [41,42], transverse resonance (like mode-matching, film mode-matching, method of lines) [43–46], variational [47], as well as wave-matching methods [48]. In our problem, the calculation of the fundamental hybrid guided modes of the dielectric circular sectoral waveguide was done by using the Circular Harmonic Function Expansion Method in combination with the Point Matching Method (PMM), as PMM is suitable for cylindrical coordinates, as well as very easy and fast for the modeling of circular sectoral mode solving. We have to note that PMM is a standard mode-solver method, firstly used by Goell [49] for the investigation of guided modes of a rectangular dielectric waveguide, while it has been applied effectively to more complex waveguide structures and confirmed experimentally as well [27,35,50–52]. In advance, numerous applications of PMM are encountered in the context of electromagnetic scattering [53]. Concerning the precision efficiency of the method, according to Ref. [40], a normal mode optical rigorous solver method should be able to provide exact three-digit values for normalized propagation constant (error less that 10^{-3}). In our case, the above-mentioned limit is satisfied, as we apply the PMM by using the Singular Value Decomposition (SVD) method for optimum mode solving, while our results were compared with preceding works in the limit of zero curvature [49]. Field convergence is achieved, even in cases where the curvature of sectoral waveguide is increased enough.

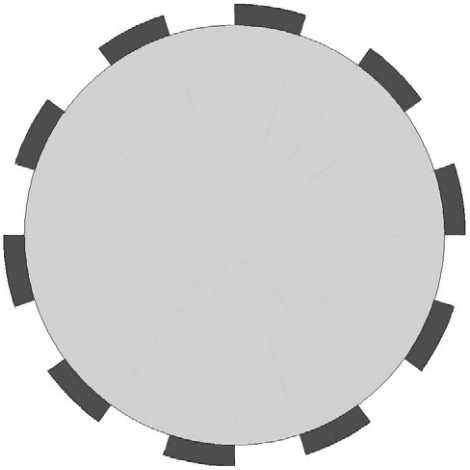

Fig. 1. The cross-section of the proposed coupler.

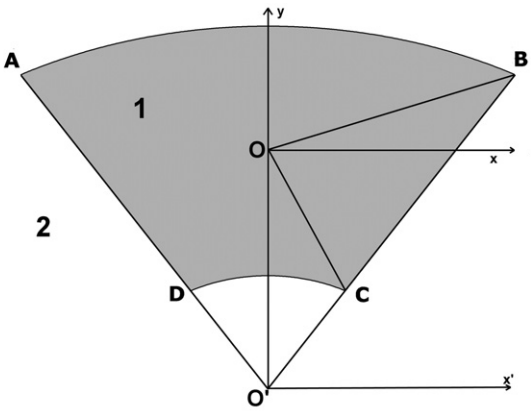

Fig. 2. The cross-section of a circular sectoral dielectric waveguide. The interior of shape ABCD constitutes the core of the ring sector.

2. Guided modes of circular sectoral dielectric waveguide

The cross-section of the proposed dielectric coupler is appeared in Fig. 1. All linear coupling coefficients between the several cores as well as Kerr coefficients can be derived using Coupled Mode Theory [1], while the fundamental modes of homogenous circular dielectric waveguide have been well investigated [54]. In this section, we will focus on the derivation of the sectoral waveguide hybrid guided modes.

In Fig. 2, we consider the sectoral core (interior of ABCD shape) isolated in the space. For our problem, we define the following geometrical parameters:

$$\begin{aligned} &ft = \angle BO'y, \quad R_{\text{in}} = O'C, \quad R_{\text{out}} = O'B, \\ &fc_1 = \angle BOx, \quad fc_2 = \angle COx, \\ &A_{\text{dim}} = ft(R_{\text{out}} + R_{\text{in}}), \quad B_{\text{dim}} = R_{\text{out}} - R_{\text{in}}, \\ &L = A_{\text{dim}}/B_{\text{dim}} \end{aligned} \tag{1}$$

Sectoral cross-section structure is determined only by ft, R_{in} and R_{out} parameters. The problem was solved for $fc_1 > 0$ and $fc_2 > ft$, while the aspect ratio parameter L ranged from 1/4 to 4/1.

In addition, n_1 and n_2 are the refractive index of core and cladding (Region 1 and 2 correspondingly in Fig. 2) with $n_1 > n_2$, $k_0 = \omega/c$ is the wavenumber in free space, ω: circular frequency of optical radiation, c: light velocity in free space, while for both regions $\mu = \mu_0$. In the framework of hybrid mode solving, the longitudinal components of the electric and magnetic field must satisfy the wave equation:

$$(\nabla_t^2 + k_n^2)\begin{Bmatrix} E_z \\ H_z \end{Bmatrix} = 0 \quad \text{with } n = 1, 2 \tag{2}$$

where $\nabla_t^2 = 1/\rho\partial/\partial\rho(\rho\partial/\partial\rho) + 1/\rho^2\partial^2/\partial\varphi^2$ and (ρ, φ, z) are the cylindrical coordinates over the O origin. Next, we use the circular harmonic expansion to write E_z and H_z components as follows:

$$\begin{aligned}
E_{z1} &= \sum_{n=0}^{\infty}[A_{n1}\sin(n\theta) + B_{n1}\cos(n\theta)]\mathrm{J}_n(k_1\rho)\exp(\mathrm{j}\omega t - \mathrm{j}\beta z)\\
E_{z2} &= \sum_{n=0}^{\infty}[A_{n2}\sin(n\theta) + B_{n2}\cos(n\theta)]K_n(\mathrm{j}k_2\rho)\exp(\mathrm{j}\omega t - \mathrm{j}\beta z)\\
H_{z1} &= \sum_{n=0}^{\infty}[C_{n1}\sin(n\theta) + D_{n1}\cos(n\theta)]\mathrm{J}_n(k_1\rho)\exp(\mathrm{j}\omega t - \mathrm{j}\beta z)\\
H_{z2} &= \sum_{n=0}^{\infty}[C_{n2}\sin(n\theta) + D_{n2}\cos(n\theta)]K_n(\mathrm{j}k_2\rho)\exp(\mathrm{j}\omega t - \mathrm{j}\beta z)
\end{aligned} \tag{3}$$

where β is the propagation constant of the guided mode, J_n is the Bessel function of first kind, K_n is the modified Bessel function of second kind, $k_1^2 = n_1^2k_0^2 - \beta^2$ and $k_2^2 = n_2^2k_0^2 - \beta^2$, while $k_1 > \beta > k_2$. Coefficients A_n, B_n, C_n and D_n, along with β are to be determined. We also define the normalized optical frequency as $V = B_{\dim}\sqrt{n_1^2 - n_2^2}k_0/\pi$ and the effective refractive index as $n_{\text{eff}} = \sqrt{(n_1^2 - n_2^2)B + n_2^2}$, where B is the normalized propagation constant, while $\beta = n_{\text{eff}}k_0$, $n_2 < n_{\text{eff}} < n_1$ and $0 < B < 1$.

Transverse components E_ρ, E_φ, H_ρ, H_φ, can be derived using Maxwell's equations, and can be expressed as functions of longitudinal components of the electromagnetic field. Furthermore, tangential components on the dielectric interface of Region 1 and 2 are expressed as linear functions of transverse components. The interface conditions imposed on fields are the continuation of tangential field components on the boundary. It is obvious that dielectric sectoral waveguide constitutes a birefrigent optical waveguide and polarization degeneracy is expected.

In order to derive the fundamental guided modes of the sectoral waveguide we have to choose a finite number of basis functions in Eq. (3), in combination with a finite number of matching points on the interface to apply the boundary conditions. In Eq. (3) by choosing $n = 0, 1, \ldots, N$ the number of unknown coefficients A_n, B_n, C_n and D_n becomes $8N + 4$, while by selecting $2N + 1$ matching points on the interface of Region 1 and 2 the number of boundary conditions are also $8N + 4$. In this way, a $(8N + 4) \times (8N + 4)$ linear homogenous system is constructed. The point-matching distribution on the dielectric interface was done by using the following formula:

$$f_i = [2\pi/(2N + 1)]i \tag{4}$$

where f_i is the angle of the matching point at the local coordination system $\mathrm{O}(\rho, \varphi)$ and $i = 1, \ldots, 2N + 1$. In order to determine the coefficients A_n, B_n, C_n and D_n, and the propagation constant β (or equivalently B) for a given set of parameters $(n_1, n_2, c, f, e_0, m_0, N, ft, R_{\text{in}}, R_{\text{out}})$, the determinant of the linear system matrix must be vanished to obtain the nontrivial solutions of the problem (guided modes). Let us note that no symmetry was applied to the system, and matching points were chosen over the whole periphery of the boundary in order to check method's validity. Indeed, the solution of the linear system provided both 'x' and 'y' modes as it will be shown next.

For best accuracy, the SVD method was applied to achieve the desired precision. SVD method offers a pole-free way for solving homogenous matrix equations. Kremer [55] have applied it to a dual-core active dielectric coupler. In our work, SVD is adopted to the PMM to avoid numerical errors for the calculation of propagation constants and mode distributions.

By increasing the number N of basis functions, we achieve convergence of the normalized propagation constant B for a given set of the parameters of the problem. To obtain dispersion diagrams, we vary the normalized optical frequency V from 0 to 4. Following the formalism used in Ref. [52], for the guided modes E_{11}^y, E_{11}^x, E_{21}^x and E_{12}^x by increasing V, the error in the estimation of B drops from 0.004 (at $V = 0.75$) to 0.0001 (at $V = 4$), while the ratio L was kept constant to unity. In Fig. 3, dispersion characteristics of a sectoral waveguide with $n_1 = 1.5$, $n_2 = 1$, $ft = 30°$, L=1 are shown, while in Table 1 we present the convergence of B for an increasing number N of basis functions at $V = 2$ for the same sectoral waveguide (E_{11}^y mode). In this table it is obvious that PMM achieves

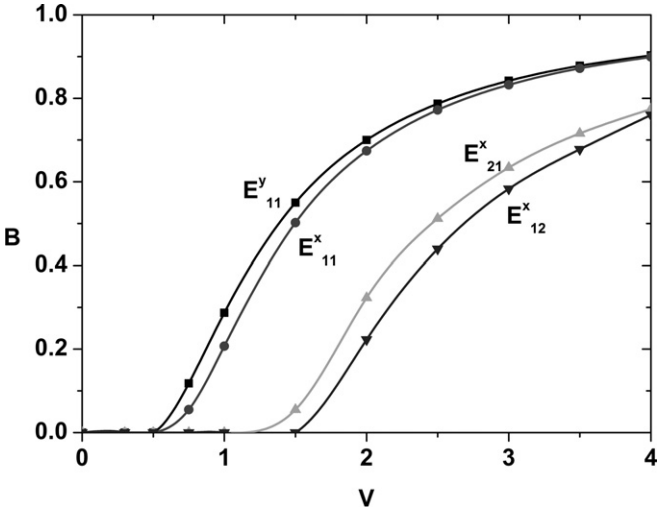

Fig. 3. Normalized propagation constant B of the first four guided modes of the circular sectoral waveguide; $ft = 30°$, $L = 1$.

Table 1
Demonstration of PMM convergence

N	B
3	0.6991
4	0.7015
5	0.7011
6	0.7006
7	0.7002
8	0.7000
9	0.7007
10	0.6997
11	0.7000

Convergence of B for an increasing N for a sectoral dielectric waveguide; $n_1 = 1.5$, $n_2 = 1$, $ft = 30°$, $L = 1$, $V = 2$, mode E^y_{11}.

0.0003 precision for B, while for the maximum number ($N = 11$) of basis functions, the execution time in a Pentium 3 PC was well below than 1 minute.

We investigate also the linear propagation characteristics of the sectoral waveguide in relation with the cross-section curvature. For this reason, by keeping $V = 2$ and $L = 1$, and varying ft from 45° to 0.01°, we obtain the normalized propagation constant B for the first fundamental mode E^y_{11}. In Fig. 4, B is plotted versus the total angle of the sectoral. PMM is very efficient even in high curvature cross-sections (at $ft = 45°$, where sectoral is quadrantal, B error is approximately 0.0003). In the limit of $ft = 0°$ a sectoral waveguide is transformed to a rectangular one. In this case, B is estimated close enough (error no more than 0.001 in all cases) to the values that are presented in Ref. [49], even in cases where aspect ratio approaches 1/4 or 4.

E^y_{11}, E^x_{11}, E^x_{21} and E^x_{12} mode field distributions of the sectoral waveguide were derived by solving the linear problem and estimating A_n, B_n, C_n and D_n coefficients according to the normalization relation:

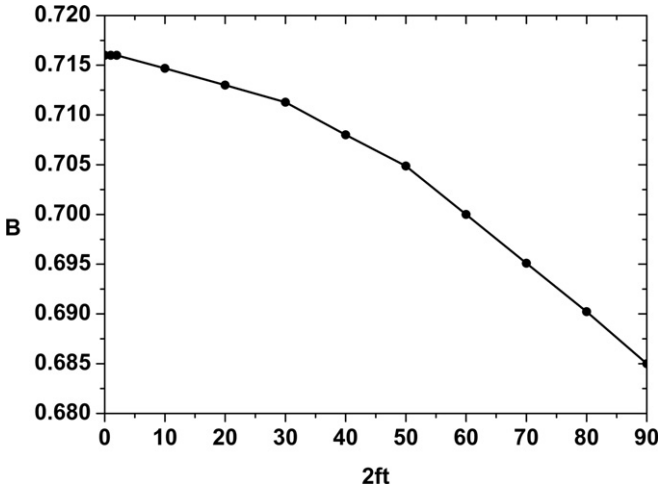

Fig. 4. Curvature dependence of normalized propagation constant B for a sectoral waveguide; $V = 2$, $L = 1$, mode E^y_{11}.

$$\int_{-\infty}^{+\infty}\int_{-\infty}^{+\infty}|F(x,y)|^2\,\mathrm{d}x\,\mathrm{d}y = 1 \quad \text{or}$$
$$\int_{0}^{2\pi}\int_{-\infty}^{+\infty}|F(\rho,\varphi)|^2\rho\,\mathrm{d}\rho\,\mathrm{d}\varphi = 1 \tag{5}$$

where $F(x,y)$ is the transverse component of the electric field, and $n_1 = 1.5$, $n_2 = 1$, $V = 2$, $ft = 30°$, $L = 1$. In Fig. 5, field distributions (magnitude of electric field) are shown for the above-mentioned modes.

In order to check the validity of the PMM, we used several distributions for the matching points on the interface. According to our second point-matching distribution, matching points were equidistant on the boundary, while in a third point distribution four of the matching points were selected exactly on the corners of the sectoral cross-section. Both distributions managed to provide results for the B close enough to the primary analysis, but they proved unstable in comparison with the distribution of Eq. (4). Thus, all results presented in next sections were derived using the point-matching distribution of Eq. (4). Furthermore, we checked PMM by shifting the origin of the xOy coordination system both at x and y-direction. In this case, again PMM was shown capable of providing the normalized propagation constant of the guided modes with an error less than 10^{-3} [40] as origin shift was below 5% and 10% of A_{dim} or B_{dim} dimensions (in x or y-direction) respectively.

An alternative way of guided mode solution was tested for the sectoral waveguide by defining four different regions at the cross-section as shown in Fig. 6. For Regions 1, 3 and 4 (cladding) the refractive index has the same value, while Region 2 constitutes the sectoral waveguide (core). A similar homogenous linear system $(24N + 12) \times (24N + 12)$ was constructed. In order to obtain the exact value of B, N had to be increased most times at very high values (15 or 17). The increased number of basis functions increased so much the order of the system that the calculation of the SVD value of the linear system matrix was extremely time consuming. However, this method provided similar results for B with moderate accuracy.

3. Linear and nonlinear coefficients of the device

Provided that the transverse profile $F(x,y)$ of a guided mode is known, the effective area of a specific guided mode can be expressed as follows [1]:

$$A_{\mathrm{eff}} = \left(\int_{-\infty}^{+\infty}\int_{-\infty}^{+\infty}|F(x,y)|^2\,\mathrm{d}x\,\mathrm{d}y\right)^2 \Big/ \int_{-\infty}^{+\infty}\int_{-\infty}^{+\infty}|F(x,y)|^4\,\mathrm{d}x\,\mathrm{d}y \tag{6}$$

while the nonlinear (Kerr) coefficient γ is defined as $\gamma = \eta_2\omega/(cA_{\mathrm{eff}})$, where $\eta_2 = 3/(8n_1)\,\mathrm{Re}(\chi^{(3)})$ is the Self-Phase Modulation (SPM) coefficient. Parameter $\chi^{(3)}$ stands for the third order susceptibility of the sectoral core. In our problem, we define also the following quantity:

$$A_r = A_{\mathrm{eff}}/[(R^2_{\mathrm{out}} - R^2_{\mathrm{in}})ft] \tag{7}$$

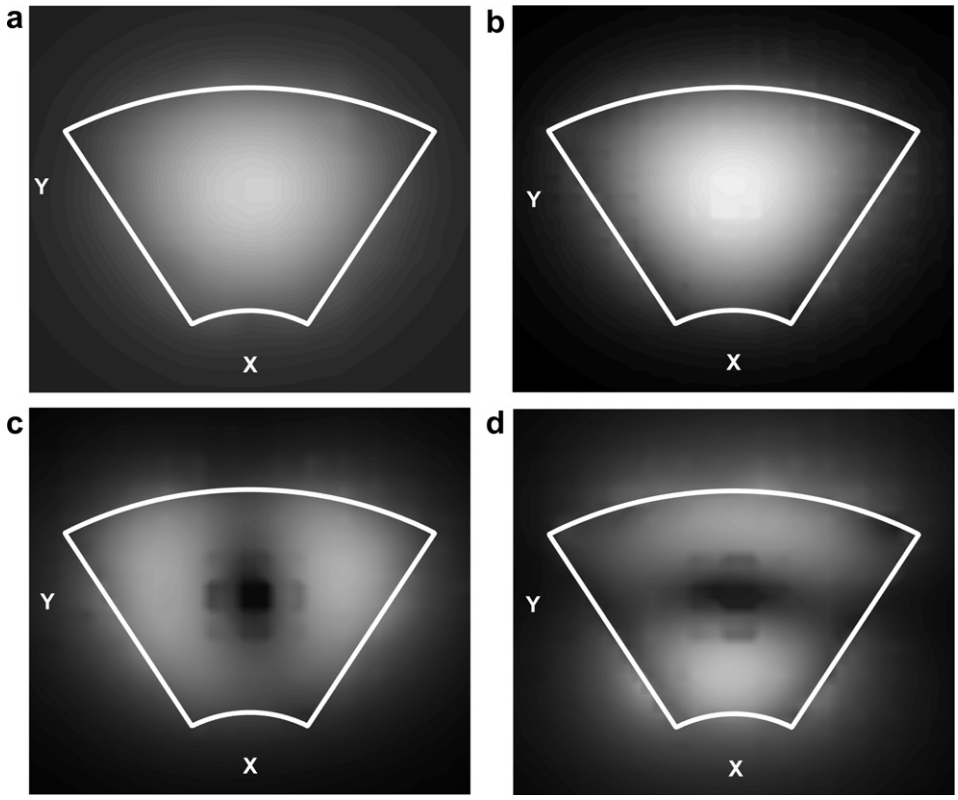

Fig. 5. Modal distribution of sectoral waveguide fundamental guided modes; $V = 2$, $ft = 30°$, $L = 1$, (a) E^y_{11}, (b) E^x_{11}, (c) E^x_{21}, (d) E^x_{12}.

which express the ratio of the effective area over the real area of the sectoral cross-section. In the case of sectoral waveguide, for the calculation of A_{eff} the integrations of Eq. (6) were executed using polar coordinates (ρ, φ) exploiting the symmetry properties of the modes, and for finite ρ to achieve convergence. In Fig. 7, A_r is plotted as a function of V (mode E^y_{11}, $n_1 = 1.5$, $n_2 = 1$, $ft = 30°$, $L = 1$). This plot shows that the mode distribution is confined into the sectoral core when normalized optical frequency is increased.

We examined also the effective area of E^y_{11} hybrid mode in relation with the curvature of the sectoral waveguide, by keeping $L = 1$ and $V = 2$ constant. Fig. 8 presents the sectoral curvature dependence of A_r. In this case, it should be mentioned that ft, R_{in}, and R_{out} were selected by keeping the aspect ratio of the sectoral waveguide constant. The corresponding curve shows that mode confinement is achieved by increasing the curvature of the sectoral waveguide. However, A_r is decreased in a complicated way

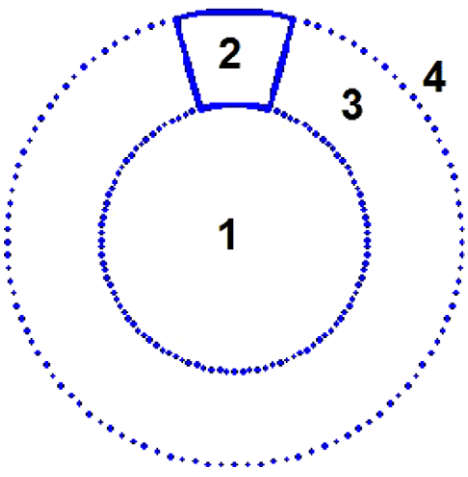

Fig. 6. Alternate point-matching distribution for mode solving of sectoral waveguide.

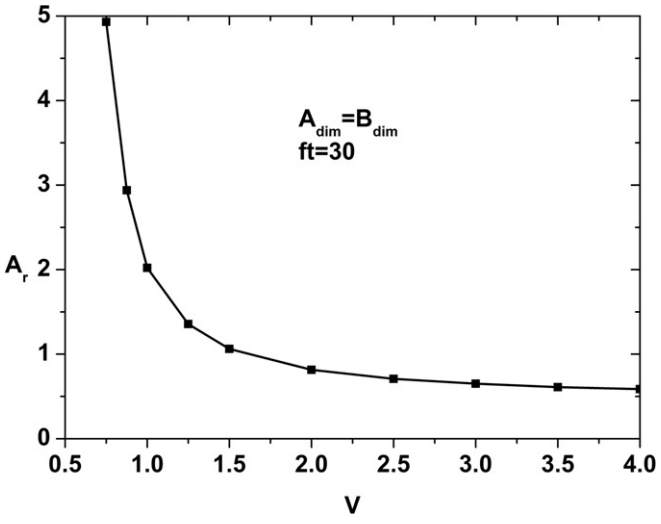

Fig. 7. Ratio A_r versus normalized optical frequency V of sectoral waveguide; mode E^y_{11}.

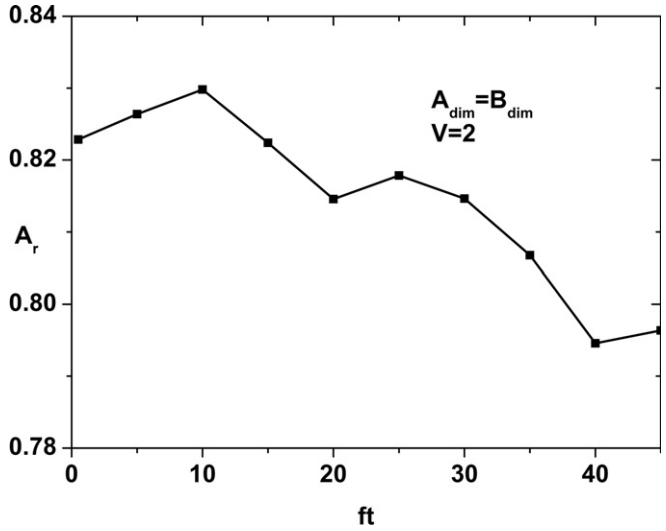

Fig. 8. Ratio A_r curvature dependence of sectoral waveguide; mode E^y_{11}.

(local maximum at approximately at $ft = 10°$ and minimum at $ft = 40°$) as ft increases because of the significant change on the sectoral cross-section.

Moreover, the linear coupling coefficient between two cores is defined by the following relation [1]:

$$\kappa_{mp} = \frac{k_0^2}{2\beta}\int_{-\infty}^{\infty}\int_{-\infty}^{\infty}\left(\tilde{n}^2 - n^2_{\mathrm{reg}\,p}\right)F_m F_p\,\mathrm{d}x\,\mathrm{d}y(m^{-1}) \tag{8}$$

where m, p: 1, 2 (correspond to first and second core), $\beta = (\beta_m + \beta_p)/2$, $\tilde{n}$ is the refractive index of the two-core coupled system, $n_{\mathrm{reg}\ p}$ is the refractive index for each core isolated in the space, F_m and F_p are the transverse profile of the corresponding mode. It is obvious that, when cores are identical, κ_{12} equals κ_{21}, while $\beta = \beta_m = \beta_p$ for the same mode.

We now consider two identical sectoral waveguides having their centers O_1 and O_2 at angular distance $dft = \angle O_1 O' O_2$ (see Fig. 9). In Fig. 10, the dimensionless parameter K, which express the normalized to unity linear coupling coefficient of two identical sectoral cores ($K = \kappa_{12}/\kappa_{\max} = \kappa_{21}/\kappa_{\max}$), is plotted versus normalized optical frequency V (mode E^y_{11}, $n_1 = 1.5$, $n_2 = 1$, $ft = 30°$, $L = 1$, $dft = 61°$). For these values of ft and dft, obviously

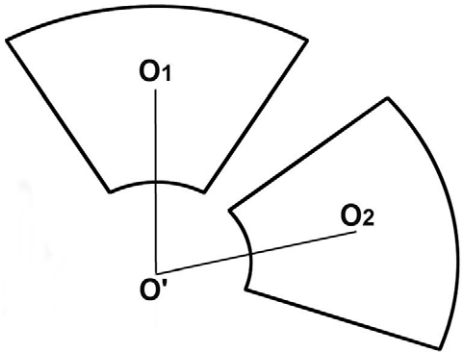

Fig. 9. Coupling between two identical sectoral waveguides.

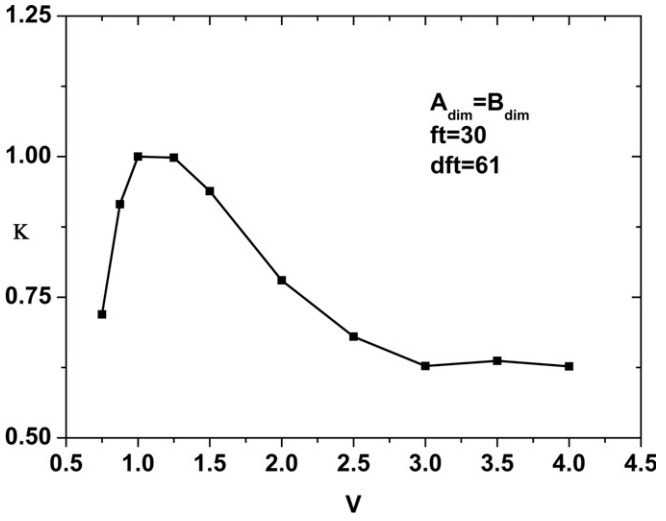

Fig. 10. Normalized linear coupling coefficient K of two identical sectoral waveguides versus normalized optical frequency V; mode E^y_{11}, $K = \kappa/\kappa_{\max}$, $\kappa_{\max} = 9.02\ \mathrm{m}^{-1}$.

the two cores are close enough (almost touching each other). For small values of V, the modes at both cores are extremely wide in space and K is small because integration in Eq. (8) is executed in the core region, where mode intensity is relatively low. When V is increased from 0 to 1.25 approximately, mode field is confined and field intensity increases. At this point, maximum field overlapping takes place providing a maximum value of K. By increasing further the parameter V, mode fields become more confined in the respective cores and field overlapping is decreased.

By keeping V constant and varying dft we obtain the K versus dft plot in Fig. 11 (mode E^y_{11}, $n_1 = 1.5$, $n_2 = 1$, $ft = 30°$, $L = 1$, $V = 2$). As expected, when the relative distance between two cores is increased, coupling phenomena attenuate in general, while exactly at $dft = 90°$, where the coupling modes have orthogonal field transverse compo-

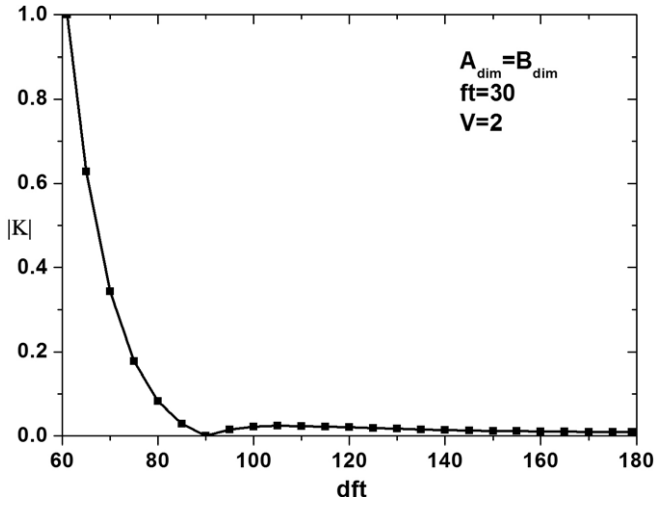

Fig. 11. Normalized linear coupling coefficient K of two identical sectoral waveguides versus dft; mode E^y_{11}, $K = \kappa/\kappa_{\max}$, $\kappa_{\max} = 7.04\ \mathrm{m}^{-1}$.

nents, coupling is diminished. In this last scenario, the sectoral waveguides deviate each other until *dft* reaches the 180° value. We checked also symmetrical cases (e.g. $dft = 179°$ and $dft = 181°$) and K error was less than 0.03%. In addition, by considering a symmetrical circular coupler consisted of 6 sectoral cores with $ft = 30°$, according to Fig. 11, for each sectoral waveguide the coupling effect, due to nearest-neighbor core ($dft = 60°$), is at least 46 times stronger than that caused by a non-neighbor waveguide ($dft = 120°$ and $dft = 180°$). For this reason, in numerous works concerning coupler arrays or lattices, only nearest-neighbor coupling is considered in planar [20–25], circular [15–18], as well as two-dimensional [26] structures.

Moreover, by keeping V and *dft* constant, and varying *ft* we obtain K versus *ft* plot in Fig. 12 (mode E_{11}^{y}, $n_1 = 1.5$, $n_2 = 1$, $dft = 61°$, $L = 1$, $V = 2$). In this last plot, it is obvious that the coupling effect is enhanced when cores of larger dimensions are being used in the coupler.

Considering now a sectoral waveguide in touch with a circular one, coupling coefficient κ_{12} and κ_{21} differ. We have calculated κ_{12} and κ_{21} using mode E_{11}^{y} for both the sectoral and the central core, the same refractive index for both cores = 1.5, refractive index of cladding = 1, and $L = 1$ for the simulations. Let us emphasize that the normalized propagation constant of E_{11}^{y} mode of sectoral waveguide is different from that of central circular core. By varying V of sectoral waveguide and keeping $ft = 30°$, we derived the normalized optical frequency as well as the transverse profile of central core mode. Thus, using Eq. (8) we produced K_{12} (central circular core coupling to sectoral one) and K_{21} (sectoral core coupling to circular waveguide) versus V (Fig. 13). Again, we observe a maximum value for both K_{12} and K_{21} approximately at $V = 1.25$. On the other hand, by varying *ft* of sectoral waveguide and keeping $V = 2$, we derived K_{12} and K_{21} versus *ft*. In Fig. 14, we observe that there is a value of *ft* (approximately at 27°) where K_{12} curve crosses K_{21} one. Let us emphasize that modeling multicore couplers of equal linear coupling coefficients is very important for the estimation of device performance in both linear and nonlinear operation.

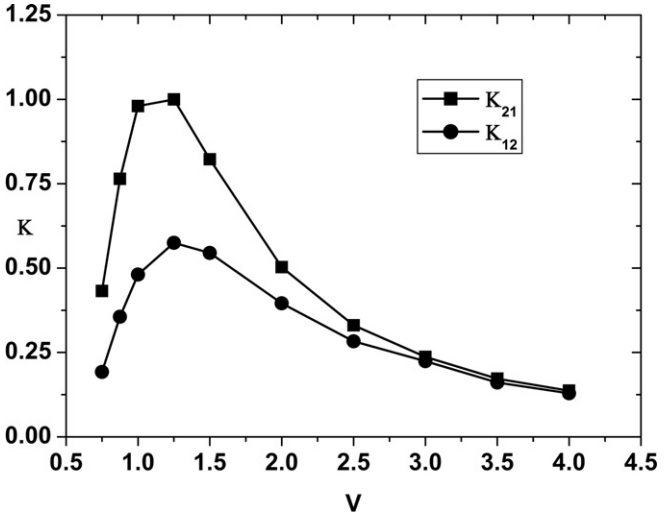

Fig. 13. Normalized linear coupling coefficient K_{21} and K_{12} between sectoral and circular waveguide versus the normalized optical frequency V of the sectoral core; $L = 1$, $n_{cores} = 1.5$, $n_{clad} = 1$, $ft = 30°$, $K_{21} = \kappa_{21}/\kappa_{21max}$, $K_{12} = \kappa_{12}/\kappa_{21max}$, $\kappa_{21max} = 22.81\ m^{-1}$, mode E_{11}^{y}.

In addition, Cross-Phase Modulation (XPM) nonlinear coefficient between two cores can be expressed as follows [1]:

$$C_{mp} = 2\eta_2 k_0 \int_{-\infty}^{\infty}\int_{-\infty}^{\infty} |F_m|^2 |F_p|^2 \,dx\,dy \quad (W^{-1}\ m^{-1}) \tag{9}$$

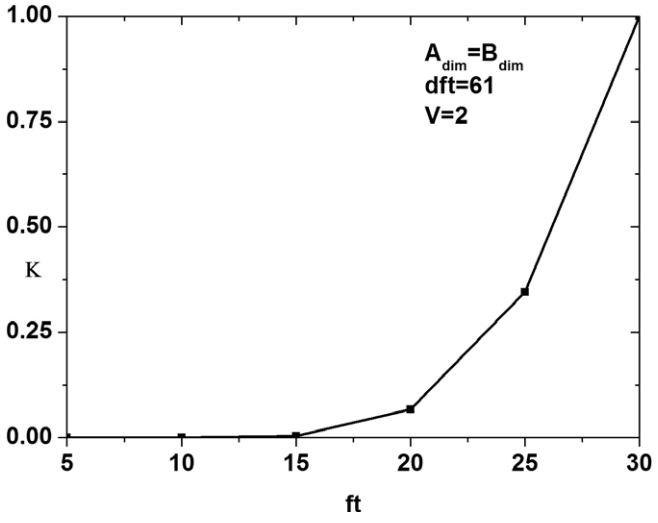

Fig. 12. Normalized linear coupling coefficient K of two identical sectoral waveguides versus sectoral core curvature; mode E_{11}^{y}, $K = \kappa/\kappa_{max}$, $\kappa_{max} = 6.98\ m^{-1}$.

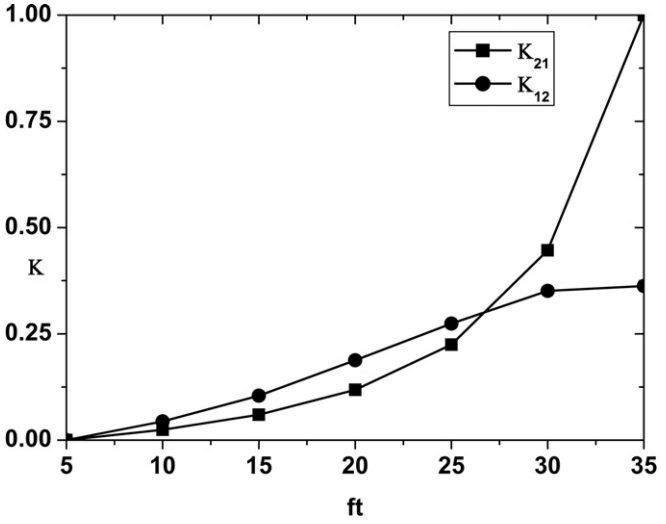

Fig. 14. Normalized linear coupling coefficient K_{21} and K_{12} between sectoral and circular waveguide versus sectoral core curvature; $L = 1$, $n_{cores} = 1.5$, $n_{clad} = 1$, $V = 2$, $K_{21} = \kappa_{21}/\kappa_{21max}$, $K_{12} = \kappa_{12}/\kappa_{21max}$, $\kappa_{21max} = 25.70\ m^{-1}$, mode E_{11}^{y}.

Table 2
Numerical example of sectoral waveguide optical parameters and coupling coefficients of the proposed coupler

Selected values	Calculated quantities
$\lambda = 1319$ nm	$L = 1$
$n_1 = 1.46$	$A_{\text{dim}} = B_{\text{dim}} = 1.24$ μm
$n_2 = 1.0$	$V = 2$
$\eta_2 = 10^{-13}$ esu	$N = 8$
$e_0 = 8.854 \times 10^{-12}$ Farad/m	$B = 0.7006$
$m_0 = 4\pi \times 10^{-7}$ Henry/m	$n_{\text{eff}} = 1.3389$
$ft = 30°$	$A_{\text{eff}} = 1.2323$ μm^2
$R_{\text{in}} = 0.564$ μm	$A_r = 0.8015$
$R_{\text{out}} = 1.804$ μm	$\gamma = 1.0136$ W^{-1} K m^{-1}
$dft = 61°$	[a] $C_{12} = 0.047457$ W^{-1} K m^{-1}
E_{11}^y mode	[b] $C = 0.007147$ W^{-1} K m^{-1}

[a] XPM coupling coefficient between sectoral and circular waveguide.
[b] XPM coupling coefficient between two identical sectoral waveguides.

where m, p, η_2, F_m and F_p have been defined in Eq. (8). Table 2 contains information about a specific example in which wavelength λ and the corresponding SPM coefficient η_2 were selected for silica fiber [56]. As it can be seen in this table, XPM coefficients are 95% smaller than γ coefficient of sectoral core. For this reason, XPM terms in a coupled DNLS or DGL equation system, which specifies the nonlinear modes (e.g. solitons) of the device, are commonly ignored.

4. Conclusion

A novel composite dielectric circular coupler was proposed where linear and nonlinear phenomena are in effect. For the first time, to the authors' knowledge, circular sectoral dielectric core hybrid guided modes were rigorously analyzed. The modal characteristics of the sectoral cores were derived using circular harmonic expansions for the longitudinal components of the electric and magnetic field in combination with the PMM. In our work, we adopted the pole-free SVD method to solve the linear modal problem concerning sectoral waveguide optical propagation. Even in cases where the curvature of the sectoral waveguide was increased, PMM was shown capable of providing satisfactory results as aspect ratio was close enough to unity. An efficient point-matching distribution was established in order to achieve normalized propagation constant convergence (B error less that 10^{-3}), even for the quadrantal sectoral waveguide case. The validity of PMM mode solver was checked for the zero curvature, the shifted origin, as well as the four-region point-matching distribution cases.

We demonstrated the birefringent characteristics of the proposed coupler deriving both 'x' and 'y' hybrid modes. Next, we focused on the effective area of the sectoral core E_{11}^y guided mode, showing that its effective area curvature dependence is quite complicated due to the significant change on the sectoral cross-section. Furthermore, many plots concerning coupling phenomena were derived in order to constitute a useful tool for the modeling of linear and nonlinear operation of the coupling device, by estimating the corresponding coefficients with significant accuracy (linear coupling coefficient error was less than 0.03% in symmetrical cases of two-sectoral coupling with origin core angular deviation $dft = 179°$ and $dft = 181°$). We also focused on optical frequency and curvature dependence of coupling effect showing regions of coupler parameters where linear coupling phenomena are enhanced, reduced or totally balanced. In the case of two-sectoral coupling, linear coupling coefficient maximum value was found in a specific region ($V \approx 1.25$) of normalized optical frequency, while in the case of linear coupling between sectoral and circular cores, it was demonstrated that linear coupling phenomena may be balanced by selecting appropriately the curvature of the sectoral core. In addition, by providing a specific example, where XPM coupling coefficients were showed to be 95% smaller than their Kerr counterparts, we verified that XPM coupling effect is in practice negligible in comparison with SPM one. We expect that this novel architecture of asymmetric, multicore and birefringent optical coupling opens a new potential in photon management applications. Moreover, adopting the SVD method, our model may be directly expanded to produce mode distributions and coupling coefficients even in cases where the refractive index of the core is complex (active or passive coupling).

Acknowledgements

This project is co-funded by the European Social Fund (75%) and National Resources (25%) – Operational Program for Educational and Vocational Training II (EPEAEK II) and particularly the Program PYTHAGORAS.

References

[1] G.P. Agrawal, Applications of Nonlinear Fiber Optics, first ed., Academic Press, San Diego, 2001.
[2] Y. Chen, J. Atai, Opt. Commun. 150 (1998) 381.
[3] B.A. Malomed, I.M. Skinner, P.L. Chu, G.D. Peng, Phys. Rev. E 53 (1996) 4084.
[4] M. Romagnoli, S. Trillo, S. Wabnitz, Opt. Quant. Electron. 24 (1992) S1237.
[5] W.B. Fraga, J.W.M. Menezes, M.G. da Silva, C.S. Sobrinho, A.S.B. Sombra, Opt. Commun. 262 (2006) 32.
[6] P.B. Hansen, A. Kloch, T. Aakjer, T. Rasmussen, Opt. Commun. 119 (1995) 178.
[7] B.A. Malomed, Phys. Rev. E 51 (1995) R864.
[8] T.I. Lakoba, D.J. Kaup, B.A. Malomed, Phys. Rev. E 55 (1997) 6107.
[9] T.I. Lakoba, D.J. Kaup, Phys. Rev. E 56 (1997) 4791.
[10] D.C. Psaila, C. Martijn de Sterke, Opt. Lett. 18 (1993) 1905.
[11] R.H. Stolen, A. Ashkin, W. Pleibel, J.M. Dziedzic, Opt. Lett. 10 (1985) 574.
[12] D. Artigas, J. Olivas, F. Dios, F. Canal, Opt. Commun. 131 (1996) 53.
[13] E.J. Bochove, P.K. Cheo, G.G. King, Opt. Lett. 28 (2003) 1200.
[14] P. Glas, M. Naumann, A. Schirrmacher, Th. Pertsch, Opt. Commun. 151 (1998) 187.
[15] K. Hizanidis, S. Droulias, I. Tsopelas, N.K. Efremidis, D.N. Christodoulides, Phys. Scr. T107 (2004) 13.
[16] K. Hizanidis, S. Droulias, I. Tsopelas, N.K. Efremidis, D.N. Christodoulides, IJBC 16 (2006) 1739.

[17] W. Krolikowski, U. Trutschel, M. Cronin-Golomb, C. Schmidt-Hattenberger, Opt. Lett. 19 (1995) 320.
[18] C. Schmidt-Hattenberger, U. Trutschel, R. Muschall, F. Lederer, Opt. Commun. 82 (1991) 461.
[19] M. Wrage, P. Glas, D. Fischer, M. Leitner, N.N. Elkin, D.V. Vysotsky, A.P. Napartovich, V.N. Troshchieva, Opt. Commun. 205 (2002) 367.
[20] D.N. Christodoulides, R.I. Joseph, Opt. Lett. 13 (1988) 794.
[21] N.K. Efremidis, D.N. Christodoulides, Phys. Rev. E 65 (2002) 056607.
[22] N.K. Efremidis, D.N. Christodoulides, Phys. Rev. E 67 (2003) 026606.
[23] H.S. Eisenberg, Y. Silberberg, Phys. Rev. Lett. 81 (1998) 3383.
[24] Y.S. Kivshar, Opt. Lett. 18 (1993) 1147.
[25] C. Schmidt-Hattenberger, U. Trutschel, F. Lederer, Opt. Lett. 16 (1991) 294.
[26] T. Pertsch, U. Peschel, F. Lederer, J. Burghoff, M. Will, S. Nolte, A. Tünnermann, Opt. Lett. 29 (2004) 468.
[27] E. Yamashita, K. Atzuki, R. Kuzuya, IEEE Trans. MTT 28 (1980) 986.
[28] R.F. Harrington, Time-Harmonic Electromagnetic Fields, first ed., McGraw-Hill Book Company, New York, 1961 (Chapter 5).
[29] A. Elsherbeni, D. Kajfez, S. Zeng, IEEE Ant. Prop. Mag. 33 (1991) 20.
[30] S. Amari, S. Catreux, R. Vahldieck, J. Bornemann, IEEE Trans. MTT 46 (1998) 479.
[31] U. Balaji, R. Vahldieck, IEEE Trans. MTT 44 (1996) 1183.
[32] U. Balaji, R. Vahldieck, IEEE Trans. MTT 46 (1998) 191.
[33] A.S. Omar, A. Jostingmeier, C. Rieckmann, S. Lutgert, IEEE Trans. MTT 42 (1994) 2139.
[34] A.W. Snyder, X.-H. Zheng, JOSA A 3 (1986) 600.
[35] Y-H. Wang, C. Vassalo, Opt. Lett. 14 (1989) 1377.
[36] V. Rastogi, K.S. Chiang, Opt. Lett. 26 (2001) 491.
[37] A. Yeung, K.S. Chiang, V. Rastogi, P.L. Chu, G.D. Peng, Opt. Fib. Commun. Conference, vol. 2, 2004, ThI4.
[38] A. Millo, I. Naeh, Y. Lavi, A. Katzir, Appl. Phys. Lett. 88 (2006) 251101.
[39] K.S. Chiang, Opt. Quant. Electron. 26 (1994) S113.
[40] C. Vassallo, Opt. Quant. Electron. 29 (1997) 95.
[41] K.S. Chiang, JLT LT-4 (1986) 980.
[42] J.E. Sader, JOSA A 7 (1990) 2094.
[43] H. Diestel, IEEE J. Quant. Electron. QE-20 (1984) 1288.
[44] S.T. Peng, A.A. Oliner, IEEE Trans. MTT 29 (1981) 843.
[45] A.S. Sudbo, Pure Appl. Opt. 2 (1993) 211.
[46] A.S. Sudbo, Pure Appl. Opt. 3 (1994) 381.
[47] W. Huang, H. Haus, JLT 9 (1991) 56.
[48] M. Lohmeyer, Opt. Quant. Electron. 29 (1997) 907.
[49] J.E. Goell, Bell Syst. Tech. J. 48 (1969) 2133.
[50] S. Gaal, E. Lorincz, P.I. Richter, M. Barabas, Opt. Commun. 155 (1998) 368.
[51] C. Vassallo, JLT 8 (1990) 1723.
[52] E. Yamashita, K. Atzuki, O. Hashimoto, K. Kamijo, IEEE Trans. MTT 27 (1979) 352.
[53] F.M. Kahnert, J. Quantit. Spectr. Radiat. Transf. 79–80 (2003) 775.
[54] H.-G. Unger, Planar Optical Waveguides and Fibres, Oxford University Press, Oxford, 1977 (Chapter 4).
[55] D. Kremer, Electron. Lett. 30 (1994) 1088.
[56] R.L. Sutherland, Handbook of Nonlinear Optics, first ed., Marcel Dekker, New York, 1996, p. 464.